AFRL-AFOSR-VA-TR-2024-0038

Multilayer, Multimaterial, Multifunctional, Thermo-structural Coatings

Sampath, Sanjay
THE RESEARCH FOUNDATION OF STATE UNIVERSITY OF NEW YORK
WEE 5510 FRK MEL LIB
STONY BROOK, NY, 117940001
US

11/27/2023
Final Technical Report

Air Force Research Laboratory
Air Force Office of Scientific Research
Arlington, Virginia 22203
Air Force Materiel Command

REPORT DOCUMENTATION PAGE

PLEASE DO NOT RETURN YOUR FORM TO THE ABOVE ORGANIZATION.

1. REPORT DATE	2. REPORT TYPE	3. DATES COVERED	
20231127	Final	START DATE 20180129	END DATE 20220128

4. TITLE AND SUBTITLE
Multilayer, Multimaterial, Multifunctional, Thermo-structural Coatings

5a. CONTRACT NUMBER	5b. GRANT NUMBER	5c. PROGRAM ELEMENT NUMBER
	FA9550-18-1-0118	61102F
5d. PROJECT NUMBER	**5e. TASK NUMBER**	**5f. WORK UNIT NUMBER**

6. AUTHOR(S)
Sanjay Sampath

7. PERFORMING ORGANIZATION NAME(S) AND ADDRESS(ES)
THE RESEARCH FOUNDATION OF STATE UNIVERSITY OF NEW YORK
WEE 5510 FRK MEL LIB
STONY BROOK, NY 117940001
US

8. PERFORMING ORGANIZATION REPORT NUMBER

9. SPONSORING/MONITORING AGENCY NAME(S) AND ADDRESS(ES)	10. SPONSOR/MONITOR'S ACRONYM(S)	11. SPONSOR/MONITOR'S REPORT NUMBER(S)
Air Force Office of Scientific Research 875 N. Randolph St. Room 3112 Arlington, VA 22203	AFRL/AFOSR ION	AFRL-AFOSR-VA-TR-2024-0038

12. DISTRIBUTION/AVAILABILITY STATEMENT
A Distribution Unlimited: PB Public Release

13. SUPPLEMENTARY NOTES

14. ABSTRACT
In this report are reflected the activities performed in the collaborative project between researchers in USA (Stony Brook University) and their counterparts in Mexico (CIATEQ and CIDESI Research Centers). The US activity was sponsored by AFOSR while the Mexican
activities were sponsored by CONACYT the Mexican research organization. The project sought to conduct fundamental scientific investigations on multilayer thermo-structural coatings used in aerospace propulsion engines. Due sustained high temperature operation of aero engines in harsh environments, coatings undergo various failure modes from mechanical fracture to oxidation to sand induced erosion and delamination. Multilayers are sought to select and apply different types of materials that would mitigate location specific distress of coatings. This requires significant development of underlying fundamental science in multilayer mechanics for coating design, materials attribute and processing. The Stony Brook- Mexico team through complementary expertise aims to build a scientific foundation and tools for a continuous collaboration. The technical development of the project was guided by the activities reflected in the 3-year work schedule described in the project proposal where a balanced effort between modeling, coating preparation and testing were proposed. These activities have been performed with Thermal and Environmental barrier coating systems. In
the section below are shown the completed activities and the outsourcing of the results obtained in the form of published papers, conferences, and awards

15. SUBJECT TERMS

16. SECURITY CLASSIFICATION OF:			17. LIMITATION OF ABSTRACT	18. NUMBER OF PAGES
a. REPORT U	b. ABSTRACT U	c. THIS PAGE U	SAR	28

19a. NAME OF RESPONSIBLE PERSON	19b. PHONE NUMBER *(Include area code)*
STACY MANNI	0000 0000

Standard Form 298 (Rev.5/2020)
Prescribed by ANSI Std. Z39.18

FINAL PROGRESS REPORT AFOSR Grant: **FA9550-18-1-0118**

Multimaterial, Multilayer, Multifunctional Thermo-Structural Coatings

Principal Investigators: Sanjay Sampath, Stony Brook University, New York, USA

Gerardo Trapaga: Ciateq, National Research Center, Mexico

Abstract

In this report are reflected the activities performed in the collaborative project between researchers in USA (Stony Brook University) and their counterparts in Mexico (CIATEQ and CIDESI Research Centers). The US activity was sponsored by AFOSR while the Mexican activities were sponsored by CONACYT the Mexican research organization. The project sought to conduct fundamental scientific investigations on multilayer thermo-structural coatings used in aerospace propulsion engines. Due sustained high temperature operation of aero engines in harsh environments, coatings undergo various failure modes from mechanical fracture to oxidation to sand induced erosion and delamination. Multilayers are sought to select and apply different types of materials that would mitigate location specific distress of coatings. This requires significant development of underlying fundamental science in multilayer mechanics for coating design, materials attribute and processing. The Stony Brook-Mexico team through complementary expertise aims to build a scientific foundation and tools for a continuous collaboration.

The technical development of the project was guided by the activities reflected in the 3-year work schedule described in the project proposal where a balanced effort between modeling, coating preparation and testing were proposed. These activities have been performed with Thermal and Environmental barrier coating systems. In the section below are shown the completed activities and the outsourcing of the results obtained in the form of published papers, conferences, and awards

ACCOMPLISHMENTS AND TECHNICAL UPDATES

The collaborative research project between AFOSR sponsored research in the USA with complementary activities sponsored by CONACYT – the Mexican Government research agency. The project was framed in the field of high temperature coatings that are key enablers in advanced aerospace propulsion. Modern gas turbines used in both commercial and military aviation are highly complex machinery where materials are exposed to sustained high temperatures under cycling loads. Advanced engines now operate at gas temperatures which exceed the melting temperatures of the structural alloys and as such need to be protected by both ceramic insulative coatings as well as through internal cooling. These so-called Thermal Barrier Coatings based on low thermal conductivity zirconia ceramics are highly complex processed microstructures that impart unique functionalities through multilayer and porous architectures. In addition, there is an increasing evolution of ceramic matrix composites as structural substrates which require a different class of multilayer high temperature environmental barrier coatings to enable their high temperature operation.

The application driver sets forth need for critical fundamental science of high temperature ceramic materials including understanding phase attributes, interface stability, thermal stability, mechanical behavior. Given that these coatings are exposed to complex thermal gradients in a highly reactive, high temperature oxidative atmosphere, the coatings are invariably multi-layers. As such mechanics and physics of assembly of these multilayers and their durability in the environment is of scientific interest. These addressing of these attributes formed the body of objectives of the international collaboration agenda

The accomplishments of the project are presented in two different groups. i.e. Thermal Barrier Coatings (TBCs) and Environmental Barrier Coatings (EBCs). The work performed in these two subjects was done in a parallel way and it is presented in the final report separately for clarity

1. Thermal Barrier Coatings (TBCs)

Different approaches were done with to optimize multilayer barrier coatings and study the behavior of different TBCs in simulated working conditions. In this sense the analytical model of thermomechanical response of multilayered coatings based on elastic energy principles and the data base of individual coating layer properties allowed CTSR to provide CIATEQ-CIDESI with a first screening of multilayered structures candidates as that shown in the next figure (Figure 1).

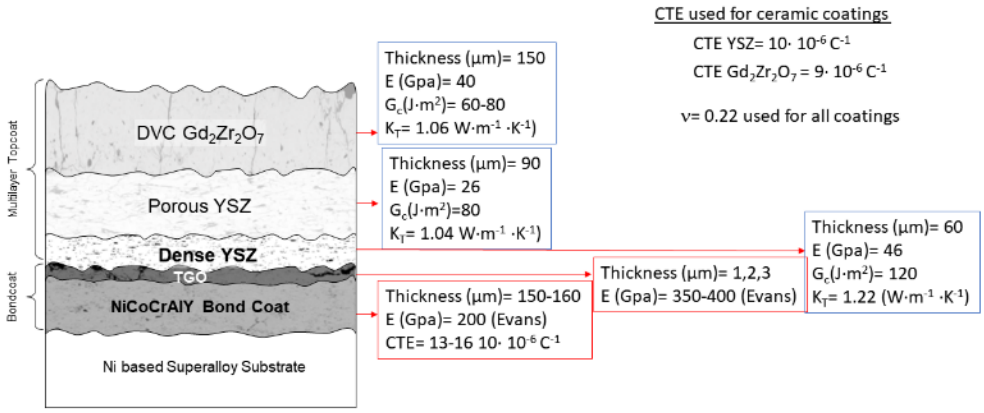

Figure 1. Scheme of one of the multilayer architectures proposed for this project reflecting the optimal thicknesses calculated considering elastic energy principles by CTSR.

CIATEQ-CIDESI extended the capabilities of well-known analytical models based on elastic energy principles to create property/failure maps for multi-layered multi-material coating architectures as those shown in the schematics of Figure 2, based in the architecture of Fig. 1. They built maps to construct and rationalize preliminary process-structure-property-performance relations for families of multi-layered architectures. Each edge of the map (shown also in Fig. 2) represents the height of each layer on the 3 layered architecture for a total thickness of that the height of the three-layered architecture is fixed to 300 microns, each edge corresponds to the fractional height of each layer. The boundary conditions for the modeling were given by the property values and minimum thickness required for each layer are shown in the table of Figure 2. The triangle formed by these dashed lines indicate the coating architectures that can be realized with the APS technique These maps were powerful tools to construct and rationalize preliminary process-structure-property-performance relations for families of multi-layered architectures.

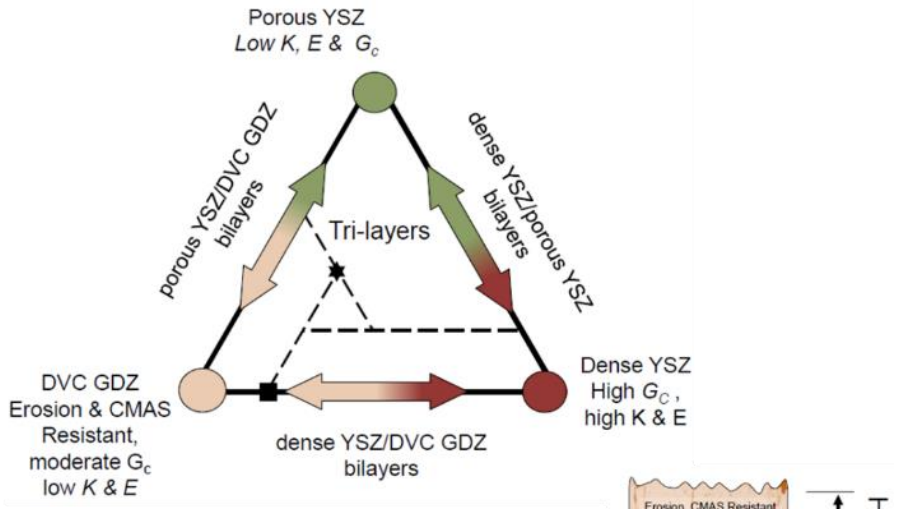

Reference APS processing window

Layer	E [MPa]	ν	$\|\alpha_s - \alpha_l\|$ [1/°C]	Gc [J/m²]	h_{min} [µm]
Dense YSZ	46×10^3	0.22	2.5×10^{-6}	90	60
Porous YSZ	26×10^3		2.5×10^{-6}	80	60
DVC GDZ	40×10^3		35×10^{-6}	60	120

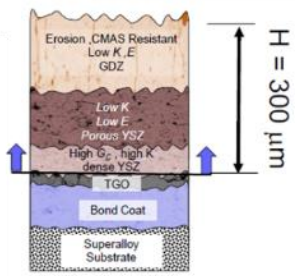

Figure 2. Scheme of one of the multilayer architectures proposed for this project reflecting the optimal thicknesses calculated considering elastic energy principles by CTSR.

CIATEQ explored the modifications required to the layered structure shown above to reduce the failure by delamination considering an isothermal cooling from temperatures close to 1000 °C to room temperature. The first result obtained from the modeling was to reduce the thickness of the stiffer layers (i.e. dense YSZ and DVC GDZ) but as reducing the total thickness of the architecture could compromise the thermal protection of the TBC, other approaches were modeled and explored. Figure 3 shows the effect of slight variations of the fracture toughness ($G_{c)}$ of each layer in the extension of the delamination resistant configuration towards the triangle area determined by the constrained total thickness of the coating and the thickness of each layer inside that architecture. Modest increments in the fracture toughness (G_c) of GDZ and dense YSZ access to delamination resistant coatings.

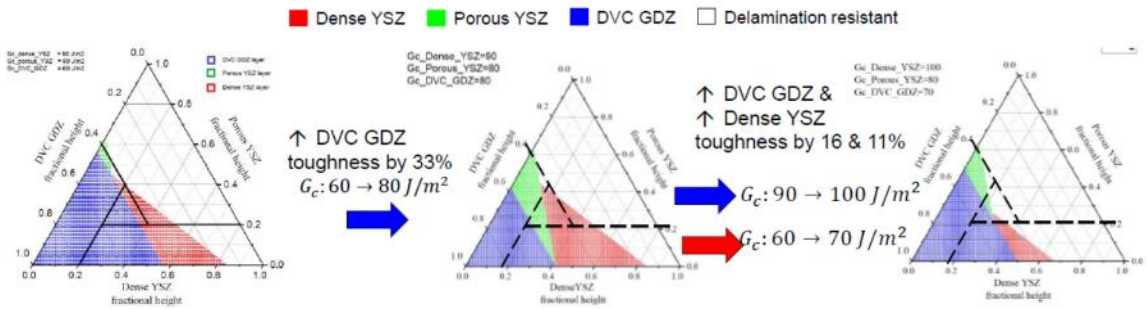

Figure 3. Enlargement of delamination resistant area produced by changes in the fracture toughness (G_c) of the coatings.

In addition to the models based on elastic energy principles, finite element simulations were out in bi-layered samples provided by CTSR. Figure 4 shows the actual microstructure of the bi-layer TBC, the schematic of the TBC on the Inconel 718 substrate and the FEM mesh used in the study. The size of the sample analyzed in this study was a 1" diameter superalloy button.

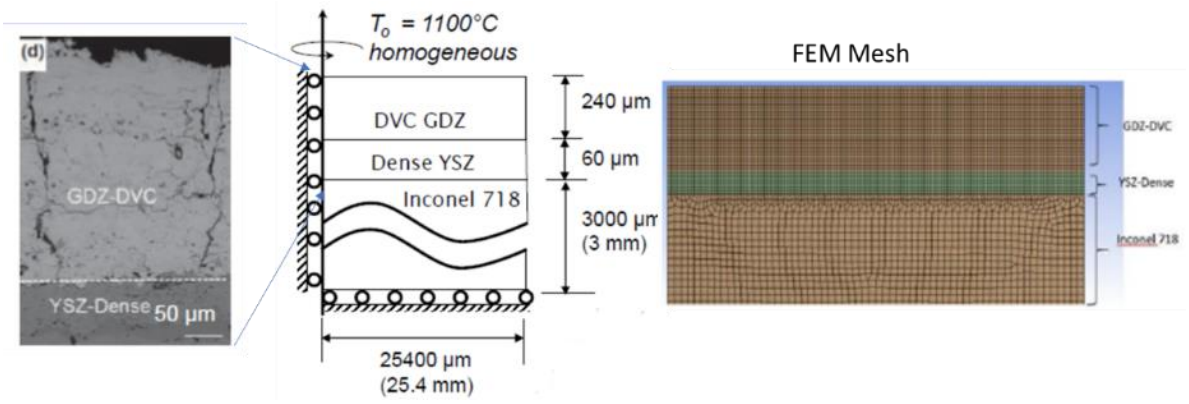

Figure 4. Microstructure, schematics and mesh of bi-layer TBC on Inconel superalloy button.

This FEM model allowed to obtain preliminary elastic energy contours as those shown in Figure 5. The highest elastic energy is stored at the edge of the sample and depends on the temperature drop of the experiment. A preliminary delamination location prediction depending on the temperature drop of in the sample is also shown in Figure 5. The higher the drop the highest the stored elastic energy. For a final temperature of 30 °C the stored elastic energy overpasses the 75 J/m^2 value at a deep of ~260 µm. The layer of the bi-layer TBC that must withstand that energy is the dense YSZ that possesses fracture toughness of ~ 90 J/m^2 which proves the beneficial of the bi-layer microstructure.

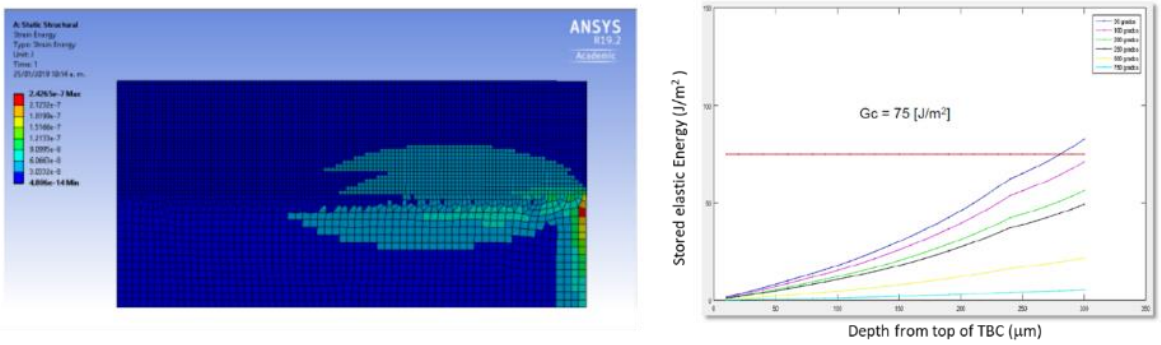

Figure 5. Elastic Energy Contours obtained by FEM modeling (left) and stored elastic energy as a function of depth from the top of bi-layer TBC of Fig.4 for different final temperatures of the system cooled from 1100 °C.

Different TBC multilayer systems were air plasma sprayed (APS) at CTSR based on the optimization of the layer thickness and character shown above. In Figure 6 are shown cross sections of some of the processed architectures

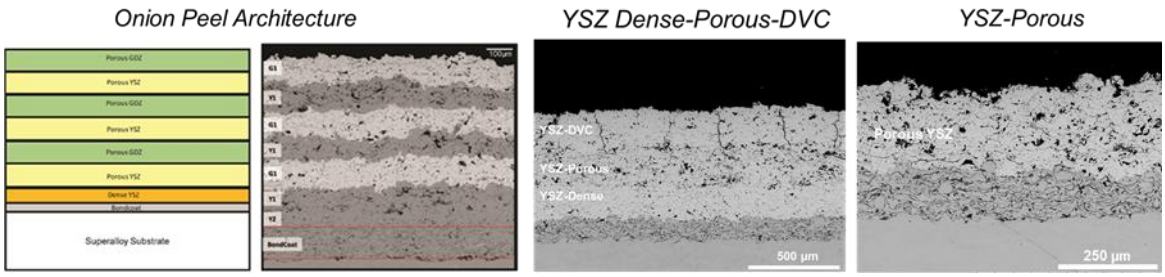

Figure 6. Example of TBC architectures processed at CTSR.

These architectures were subjected to burner rig thermal cycling and CMAS/Ash attack using the Burner Rig set up at CTSR optimized inside this project (See Fig. 7). The system allows to test TBC/Superalloy systems up to 1300 °C surface temperature. A gradient temperature is created by back cooling of the sample using compressed air. This design produces the characteristic thermal gradient present in real TBC applications. The front and back temperatures are recorded by IR Pyrometer and thermocouple respectively. The time at heating and cooling states is controlled by a pneumatic system that moves a Propane-Oxigen torch in an out the tested sample. All the parameters are registered by a LabView program.

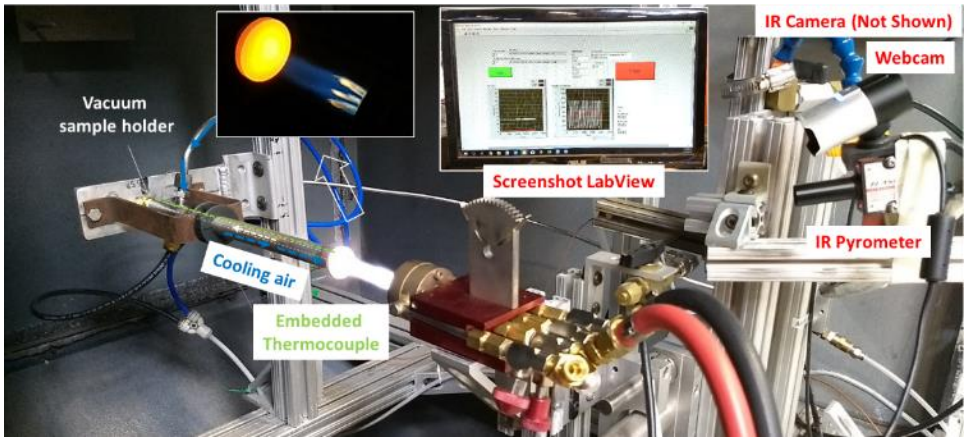

Figure 7. Burner Rig employed for thermal cycling and CMAS/Ash attack study.

Figure 8 show images recorded at different stages of the Burner Rig test. The failure mode depends on the TBC architecture

Figure 8. Images of a TBC sample at different stages of the Burner Rig test.

The 3D distribution of cracks before and after test was studied using the Computerized Tomography-SCAN (CT-SCAN) of CIDESI at CENTA (Centro Nacional de Tecnologia Aeronautica, Queretaro). The analysis was performed at two levels of resolution. In a first approach a lower level of resolution was used to study the average morphology of the layers and the interfaces between them. In Figure 9 can be seen different sections of a sample machined from a TBC system sprayed at CTSR consisting on a porous YSZ top layer a MCrAlY bond-coat and a Ni-based superalloy. The CT-scan reveals the presence of surface cracking, maybe produced during the machining of the sample. The image of the cross-section of the bond-coat shows how much denser and homogeneous is than the YSZ top-coat. This difference is easy to see using Scanning Electron Microscopy analysis but not the differences in interface microstructure that CT-Scan analysis reveals

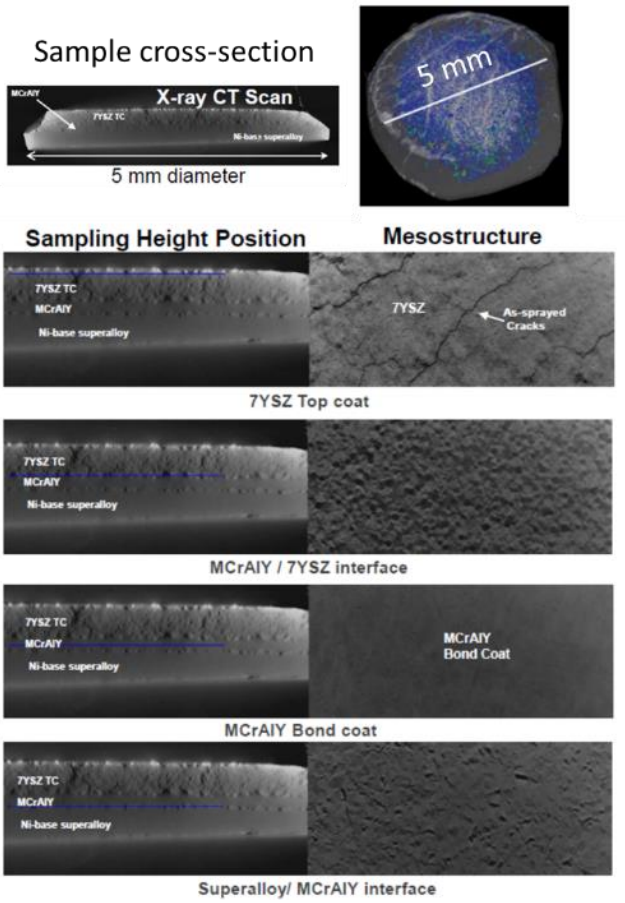

Figure 9. CT-Scan images of the different layers and layers interfaces acquired in a 5mm diameter sample machined from a porous YSZ/MCrAlY bon-coat/Ni-based superalloy substrate

The analysis at higher resolution revealed the pore distribution structure. Figure 10 shows high resolution vertical cross-sections obtained across the sample. The analysis and CT reconstruction of the acquired images revealed the presence of out-of-plane connected pores. These are features that are difficult to see through the conventional 2-D SEM analysis.

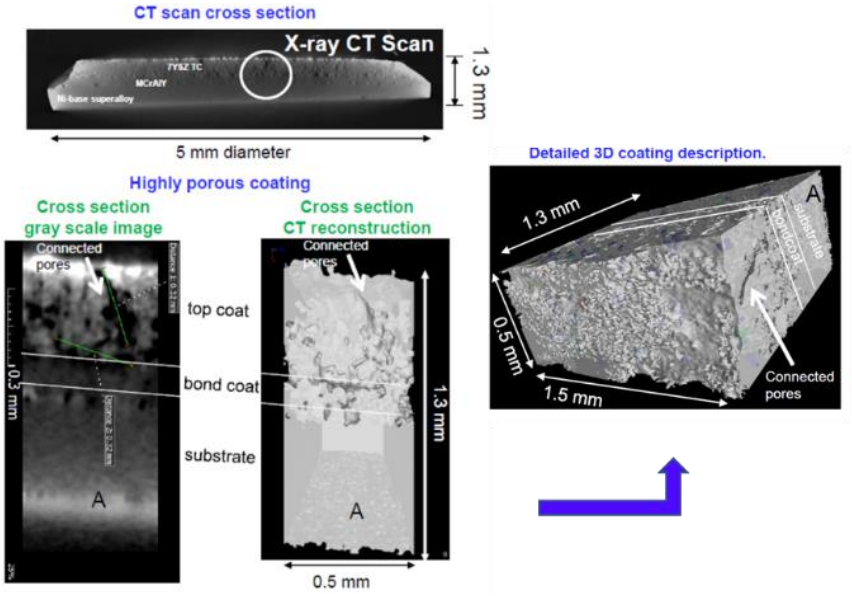

Figure 10. High resolution CT-SCAN vertical cross-section of the coating (left) and 3D image reconstructed from the obtained images

The CT-SCAN analysis opened a way for future 3D statistical characterization of the pore size and distribution that in addition to the morphology of the interfaces between layers will help to build high fidelity FEM models, stablishing connections between coating properties and 3D structure. Parameters like representative volume elements for the model and to stablish connections between coating fracture/delamination processes and structure were discovered as fundamental for the correct use of CT scan data.

Calcium-Magnesium-Aluminum-Silicate (CMAS) effect and dynamic response on TBCs was studied on two types of yttria stabilized zirconia (YSZ) microstructure [porous and dense vertically cracked (DVC)] and one gadolinium zirconate (GZO) coating (DVC), with an emphasis on understanding the incipient response of the coating surface to impacting CMAS droplets. Through both in situ video graphic observation of the interaction process on deliberately polished coating surfaces and careful ex situ microstructural analysis to examine the aftereffects, these dynamic effects of spreading/infiltration and reactions were elucidated. The microstructures of the studied TBCs are shown in Figure 11.

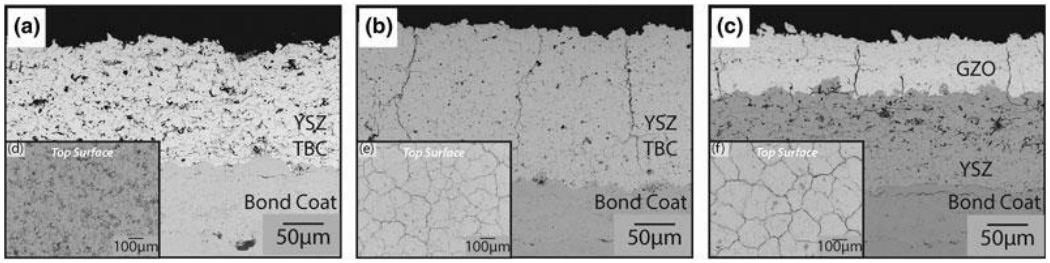

Figure 11: Representative as-deposited microstructures of (a) porous 7YSZ, (b) DVC 7YSZ, and (c) the YSZ/GZO multilayer coating with DVC GZO as the topmost layer. Inset (d–f) the respective polished top surface microstructures of the three coatings.

Figure 12 shows the three types of samples shown above during and after the CMAS test through direct imaging of the process. As noted in the experimental section, a small oxy-propane combustion flame (approximately 15 mm in diameter) was used to both heat the TBC surface and feed the CMAS particles within. CMAS particles were introduced once the surface of the coating reached a steady-state 1275 °C. The CMAS particles fed through the torch, given the nonuniform size distribution of raw Lignite Ash, were likely a mixture of molten and semi-molten particles prior to impact. As such, upon impact the droplets that were molten would spread into a disk form, transferring kinetic energy into viscous flow much in the same way as thermal spray particles impact a surface. In most thermal spray cases, it is well understood that molten particles spread before rapid solidification occurs. In the current situation unlike thermal spray, the impacted droplets continue to remain molten upon impact due to the continuous (~20 min) high surface temperature of the TBC.

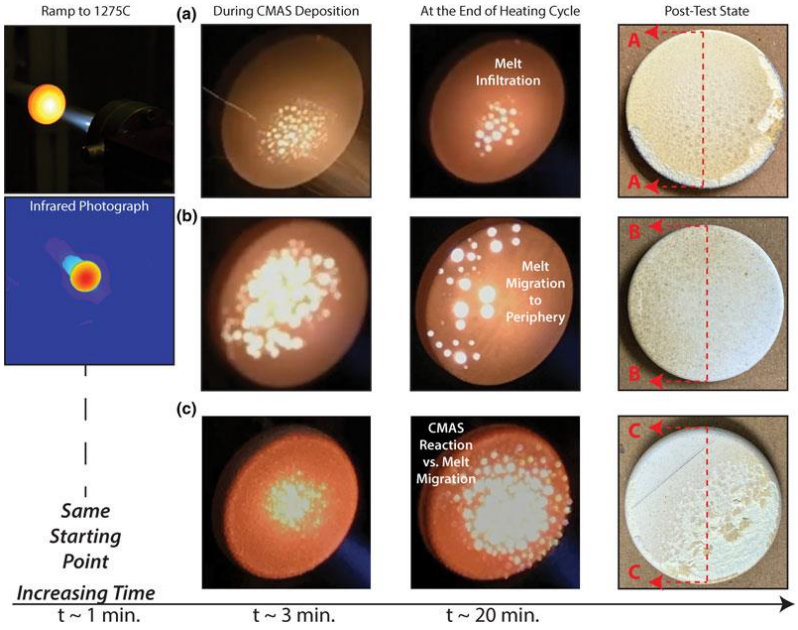

Figure 12. Time-lapse photographs of the three samples during the CMAS test. (a) Porous 7YSZ, (b) DVC 7YSZ, and (c) the YSZ/GZO multilayer coating. All samples were preheated to a surface temperature of approximately 1275 °C as measured by the pyrometer prior to the injection of CMAS. Samples were cross sectioned after testing along the line A–A/B–B/C–C for microstructural viewing.

The samples were observed by scanning electron microscopy to assess the interactions between the molten CMAS and the TBC in both surface and cross section. The study was performed in areas with different attack of CMAS (high and low). The features and microstructures found outlined allowed proposing a mechanism how molten CMAS droplets interact with different TBC materials and microstructures under dynamic impinging CMAS droplet loading via burner rig experiments. Figure 13 presents a schematic illustration of proposed interactive mechanisms between molten CMAS and TBCs of varying microstructure and chemistry. For **porous 7YSZ** TBCs exposed to CMAS within sufficiently short time scales and relatively low concentration in a burner rig gradient test, a number of effects seen in previous literature still take place. The open porosity and surface cavities on the surface can lead to melt flow instabilities for the impinging molten CMAS droplets. Furthermore, the open cavities and microcracks at the top surface (exposed from the polishing procedure) act as collection sites for the molten CMAS. As the melt wets the surface and collects within these cavities,

the connected microcrack network beneath the cavities pulls the melt in through capillary suction. While the idle CMAS melt accumulates in the depth of the TBC, further interactions such as grain boundary attack can occur. For **DVC YSZ** TBCs, the proposed mechanism for CMAS interaction is significantly different. In the case of the DVC microstructure, there are intrinsically fewer open cavities for CMAS to accumulate. Additionally, the polished surface provides a smooth surface of the CMAS to flow laterally. For DVC YSZ TBCs, the proposed mechanism for CMAS interaction is significantly different. In the case of the DVC microstructure, there are intrinsically fewer open cavities for CMAS to accumulate. Additionally, the polished surface provides a smooth surface of the CMAS to flow laterally and due to the overall amount of microcracks that this DCV architecture possesses, the suction of molten CMAS is also diminished. In the case of the **vertically cracked GZO** coating, the rapid reaction between the silicate droplet and the surface prevents the radial mobility of the droplet as in the DVC YSZ. With the CMAS droplets radially immobile, the propensity for melt flow into the DVC macro cracks of the GZO is more probable during prolonged exposure at high temperatures. It is observed due to the nature of the reactivity between GZO DVC and this Lignite Ash CMAS composition, the CMAS attack in the GZO/YSZ multilayer coating is a much more concentrated type of attack rather than what is seen in the YSZ DVC, which is more globally dispersed along the surface.

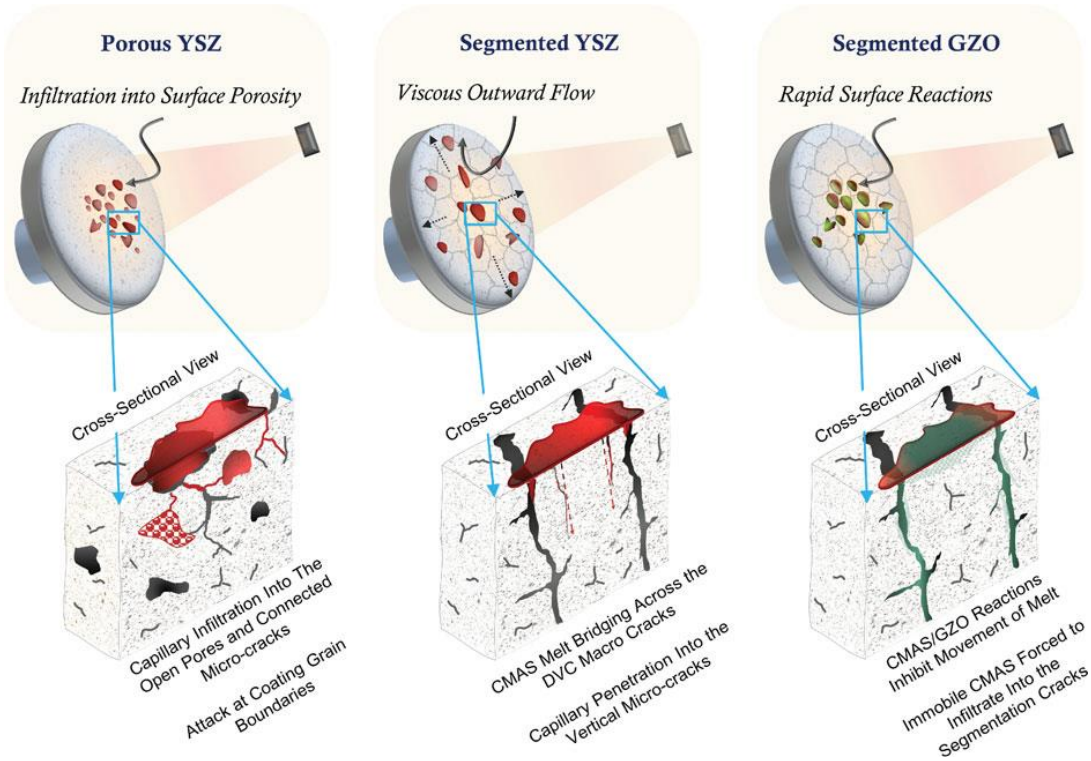

Figure 13. Proposed mechanisms of incipient interactions between CMAS particulates and TBCs of different chemistry and architecture. The interactive mechanism between CMAS and a TBC is proposed to change based on the topography, microstructure, and chemistry at the coating surface.

This work was published in 2019 (**E. Gildersleeve, V. Viswanathan, S. Sampath, "Molten Silicate Interactions with Plasma Sprayed Thermal Barrier Coatings: Role of Materials and Microstructure" Journal of European Ceramic Society 39 (2019) 2122-2131** https://doi.org/10.1016/j.jeurceramsoc.2019.01.023)

Some of the samples tested in CMAS conditions were also studied by CT-SCAN. Figure 14 shows the images recorded with this technique.

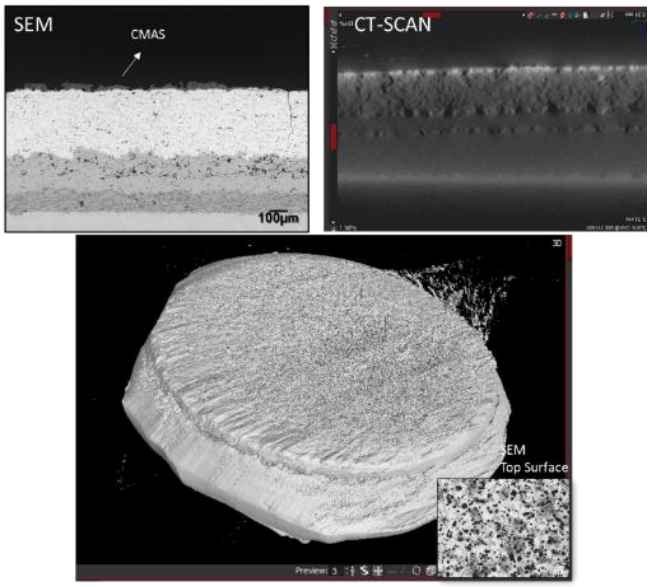

Figure 14. SEM and CT-SCAN cross sections of TBC samples with CMAS on the top-surface and CT-SCAN reconstruction

The CMAS splats were seen as bright features on the CT-SCAN 2D cross-section and as dark spots on the 3D reconstructed structure similar to that observed by SEM on the top surface of the TBC (see inset besides the 3D reconstruction).

2. Environmental Barrier Coatings (EBCs)

The work performed at CTSR with multilayer TBC was also applied to face the challenge of multilayer Environmental Barrier Coatings (EBCs). The approach that was stated in the project proposal of using Yttrium silicates was updated and improved by the use of Ytterbium silicates as top coats of EBC architectures. These architectures are formed by a bulk SiC substrate that is a reference material with similar properties to the SiC/SiC composites. These composites are difficult to obtain due to intellectual property (IP) restriction. On the SiC substrate is produced a plasma sprayed silicon (Si) bond coat and a top layer of $Yb_2Si_2O_7$, to form the EBC architecture. Fig. 15 shows the designed microstructure. Figure 15a shows the coatings in the as sprayed conditions and in Fig. 15b after a heat treatment at 1300 °C that is required to recover the crystalline nature of the coating, requisite for a better performance as EBC. The as sprayed coatings are mainly amorphous and need to be heat treated to recover the original crystallinity of the feedstock powder.

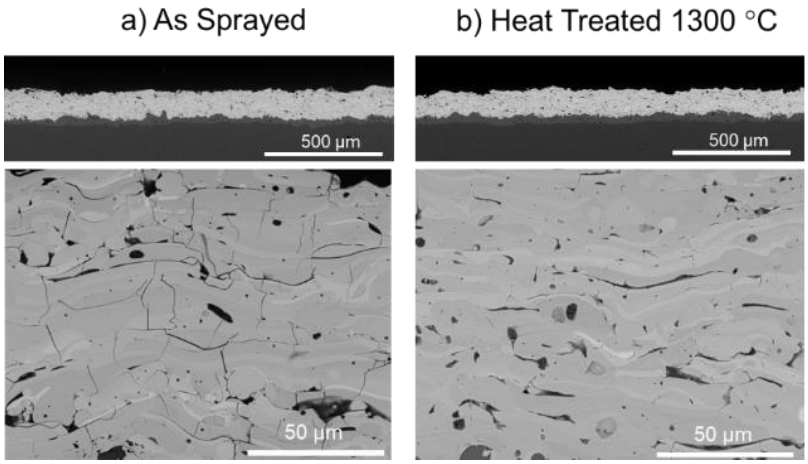

Figure 15. $Yb_2Si_2O_7$ based EBCs. SEM of the polished cross-section of a) as sprayed and b) heat treated at 1300 °C

CTSR developed in the scope of this project the right heat treatment scheme to produce EBC coatings with the right crystallinity and studied the evolution of different key properties of the coatings as the coefficient of thermal expansion (CTE). Figure 16 reflects the effect of the heat treatment on the properties and microstructure. The as sprayed coating is mainly amorphous when the temperature is increased different Yb silicate phases crystallize depending on the plasma spraying conditions as these produce a change on the final coating chemistry. The evolution of phases during crystallization produces a change in the CTE and also a crack healing effect. The findings of this work are reflected in the published work **E. Garcia, Hwasoo Lee, Sanjay Sampath "Phase and microstructure evolution in plasma sprayed $Yb_2Si_2O_7$ coatings"** ***Journal of the European Ceramic Society 39 (2019) 1477–1486.*** https://doi.org/10.1016/j.jeurceramsoc.2018.11.018

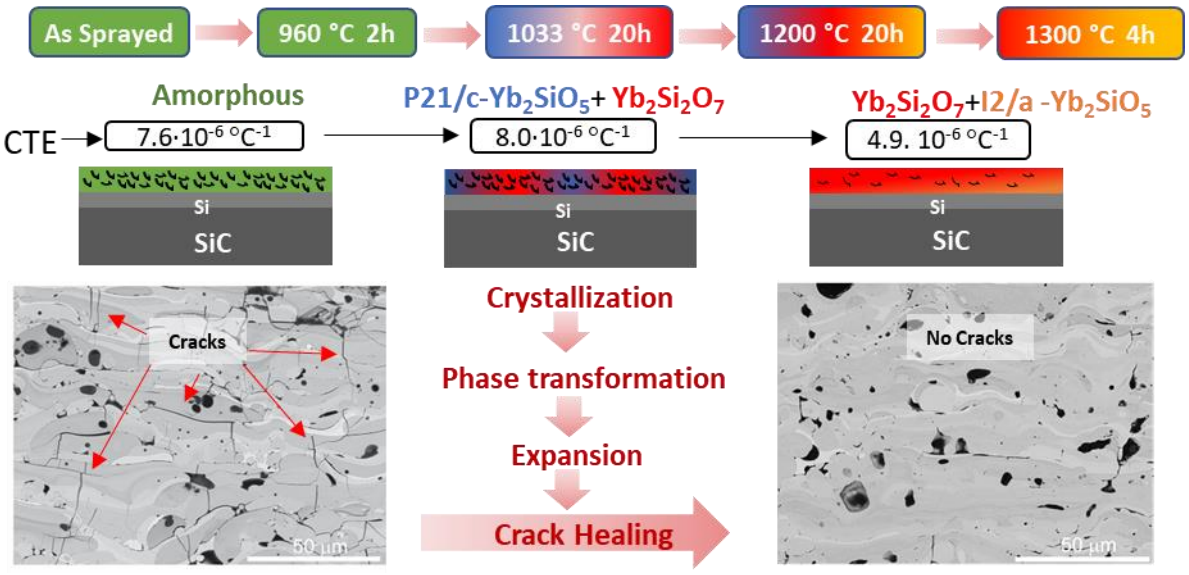

Figure 16. Effect of heat treatment on $Yb_2Si_2O_7$ EBCs phase, properties and microstructure.

Fig. 17 presents results from *in situ* XRD characterization at different temperatures of two YbDS coatings obtained using different plasma conditions; YbDS-3H (A, B) and YbDS-9H (C, D). The '3D' plot of XRD patterns in Fig. 17A and C are conveniently divided into three temperature ranges: (i) 25-900 °C, (ii) 1000- 1100 °C, and (iii) 1200- 1300 °C. The XRD patterns collected at 25 ◦C (as-sprayed), 1000 °C, 1100 °C, 1200 °C, and 1300 °C are reproduced in Fig. 17B and D for clarity, and the XRD peaks have been indexed.

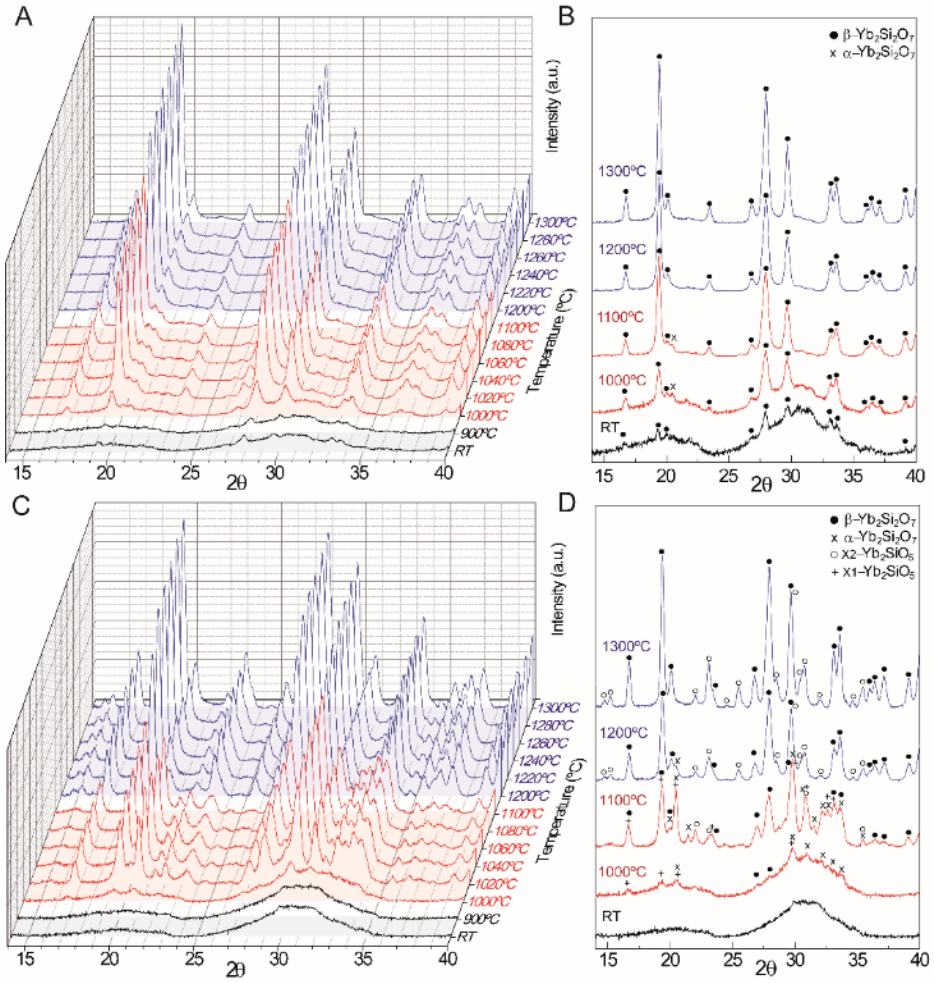

Figure 17. XRD patterns from the free-standing EBCs as a function of temperature in air: (A, B) YbDS-3H and (C, D) YbDS-9H.

The evolution of YbDS-3H EBC with temperature (Fig. 17A and B) is somewhat straightforward, where the EBC in the first temperature range is primarily amorphous. The XRD peaks assigned to the stable β-$Yb_2Si_2O_7$ phase are from unmelted particles of the feedstock powder due to the relatively low-power APS deposition. The intensities of the $Yb_2Si_2O_7$ diffraction peaks increase with temperature in the second temperature range, with the appearance of a small peak associated with the metastable α- $Yb_2Si_2O_7$ phase. The α- $Yb_2Si_2O_7$ phase disappears in the third temperature range, and β- $Yb_2Si_2O_7$ become more intense and better defined up to 1300 °C. The evolution of the YbDS-9H EBC with temperature (Fig. 17C and D) is more involved. XRD patterns show that this EBC is completely amorphous in the first temperature range. At 1000 ◦C, XRD peaks associated with the

metastable phases X1- Yb_2SiO_5 and α- $Yb_2Si_2O_7$, and the stable β- $Yb_2Si_2O_7$ phase, appear. However, note that there is significant overlap between the peaks associated with these phases. These XRD peaks intensify with increasing temperature in the second temperature range, with the appearance of peaks associated with the stable X2- Yb_2SiO_5 phase. The XRD patterns in the third temperature range show a drastic change, where only peaks associated with the stable β- $Yb_2Si_2O_7$ (majority) and X2- Yb_2SiO_5 (minority) phases remain and become more intensified and better defined (Fig. 17D).

In addition to these tests, 3D X-ray Microtomography was performed on coatings sprayed in YbDS-9H conditions (fully amorphous in as-sprayed state with a significant displacement of composition). Fig. 9A and B show 3D XRM images of pores (0.5 µm.voxel^{-1} resolution) of the as-sprayed and heat-treated (1300 ◦C, 4 h, in air) EBCs. The advantage of this 3D characterization technique over routine 2D image analysis is that the isolated (closed) and the connected porosities can be distinguished. The isolated and the interconnected porosities in the as-sprayed EBC (Fig. 19A) are estimated at 2.16 % and 1.02 %, respectively, totaling 3.18 % porosity. After heat-treatment (Fig. 19B), the isolated porosity remains about the same (2.15 %), but the interconnected porosity has increased to 3.80 %; total porosity 5.95 %. This increase in porosity corresponds to an overall linear expansion of +0.92 % (+2.77 vol%). Figs. 18C and D are 3D XRM images of pores showing pore thicknesses (diameter of the largest sphere that fits into the pore). It is seen that the interconnected pores generated after heat-treatment are quite thin (<5 µm).

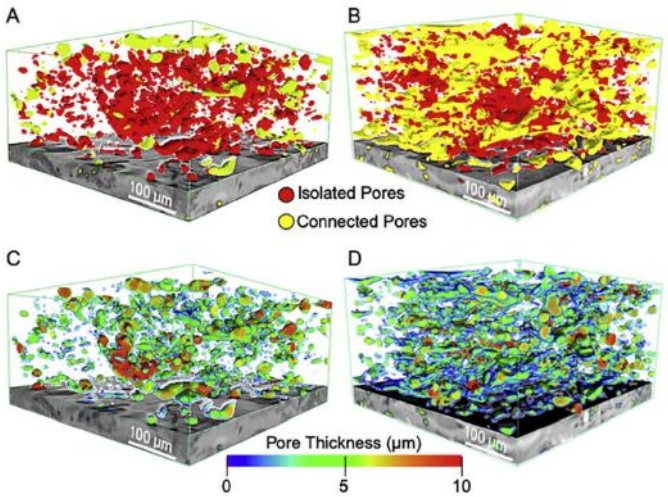

Figure 18**.** 3D XRM images of porosity and pore thickness in YbDS EBCs: (A, C) as-sprayed and (B, D) heat-treated (1300 ◦C, 4 h, air). In (A) and (B), the red regions are isolated pores and the yellow regions are interconnected pores. In (C) and (D), the color scale indicates pore thickness.

The combination of results of hot stage XRD analysis shown in Fig. 17, the porosity incremental and pore size and change measured by 3D XRD microtomography (Fig. 19) and the increase of volume of the samples measured by dilatometric techniques reported in the partial reports has resulted in a new understanding of the crystallization behavior of as-sprayed YbDS-based APS EBCs. The crystallization pathway of amorphous coatings is complex. Initially, a mixture of metastable α-$Yb_2Si_2O_7$ and X1-Yb_2SiO_5 phases form, along with stable β-$Yb_2Si_2O_7$ and X2-Yb_2SiO_5 phases. Eventually the metastable phases transform to the stable β-$Yb_2Si_2O_7$ (major) and X2-Yb_2SiO_5 (minor) phases. The significant volume expansion associated with these transformations, contributes partially towards the anomalous expansion measured in these EBCs after crystallization, but it does not

account for all the measured expansion, the porosity was also found to increase upon crystallization heat-treatment, primarily in the form of thin, interconnected pores. Thus, this phenomenon also contributes to the measured anomalous expansion. Based on this understanding, guidelines are provided for obtaining near-net-shape crystallization of phase-pure, dense β-$Yb_2Si_2O_7$ EBCs that are free of vertical cracks. More detail analysis of this study can be found in the paper, **E. Garcia a, H. F. Garces, L. R. Turcer, H. Bale, N. P. Padture, S. Sampath**. **Crystallization behavior of air-plasma-sprayed ytterbium-silicate-based environmental barrier coatings**, **Journal of the European Ceramic Society 41 (2021) 3696-3705** (https://doi.org/10.1016/j.jeurceramsoc.2020.12.051).

One important lesson learnt in this project regarding EBCs is that coatings with different SiO_2/Yb_2O_3 ratios could be obtained modifying the plasma spray conditions due to the preferential volatilization of SiO_2 during plasma spray process. Different SiO_2/Yb_2O_3 ratio is directly related with the Yb_2SiO_5 and $Yb_2Si_7O_5$ composition of the coating. In this sense a Yb-silicate coating with high amount of Yb_2SiO_5 phase (close to or greater than 50 mol%) that could be used as intermediate coating layer in a multilayered EBC architecture or as a water vapor enhanced EBC surface layer was deposited on a Si coated SiC substrate. Micro-Raman analyses were performed on as sprayed and heat treated EBC samples confirming the amorphous character and the phase differences found at different treatment temperatures. Figure 19 shows the most representative Raman spectra recorded on the coatings treated at different temperatures. The as sprayed coating (bottom of Fig. 19) does not show any peak, just three broad bands around 100, 350 and 900 cm^1 confirming its amorphous nature as it was confirmed by XRD analysis. The 1300 °C heat-treated coating shows a mixture of stable β-$Yb_2Si_2O_7$ and X_2-Yb_2SiO_5 phases which match to those detected by XRD. The spectrum recorded on the coating heat treated at 1080 °C showed notable differences, in this case the phases present in the coating are more difficult to identify as, to the extent of the authors knowledge, no experimental results of Raman shift have been reported for peaks related with metastable α- $Yb_2Si_2O_7$ and X_1-Yb_2SiO_5. We identified the phases using calculated Raman spectra reported in the literature. According to these calculations, the metastable α- $Yb_2Si_2O_7$ presents a peak at 700 cm^{-1} that corresponds to Si–O–Si stretching in the Si_3O_{10} unit and a complex shape of the high-frequency Raman peaks above 800 cm^{-1} related with asymmetric stretching of Si-O bonds and differs from the dual high-intensity peaks found for β-$Yb_2Si_2O_7$. The 700 cm^{-1} calculated peak is shifted to 732 cm^{-1} in our case, and similar displacement is found for the Raman peaks above 800 cm^{-1}. The identification of X_1- Yb_2SiO_5 was more complicated as its main intensity peaks lay above the 800 cm^{-1} region populated with the already mentioned high-frequency α- $Yb_2Si_2O_7$. What it is clear from the Figure 19 is that the high intensity peak at 887 cm^{-1} cannot be correlated with stable α- $Yb_2Si_2O_7$ though small peaks of this phase were detected in the 500-700 cm^{-1} range or with X_2-Yb_2SiO_5 as no signs of the characteristic doublet of the oxyorthosilicates B-type structure is detected. Considering that X_1-Yb_2SiO_5 is isostructural with X_1- Gd_2SiO_5 (A-type oxyorthosilicate) the Raman spectrum of this phase was used to identify the possible presence of X_1-Yb_2SiO_5. The sharp peak detected at 71 cm^{-1} is identified in Figure 19 with a question mark (?) because although it seems to be related with the X_1-Yb_2SiO_5 it has not being identified in the literature. It could be miss identify as one of the stable X_2-Yb_2SiO_5 phase but in that case (spectrum labelled in Figure 19- 1300 °C) the peak is detected at 78 cm^{-1}.

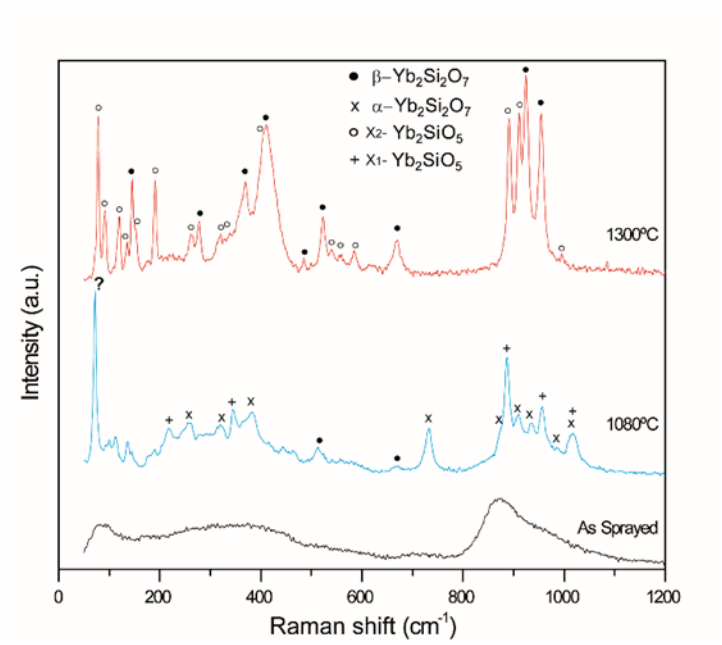

Figure 19. Raman shift spectra of as spray and heat-treated EBC One-Layer EBC coating at 1080 and 1300 °C.

The crystallization treatments produced a continuous change of thermal expansion coefficient from the amorphous state to the fully crystallized coating. Figure 20 shows a typical behavior of the relative thermal expansion of a $Yb_2SiO_5/Yb_2Si_2O_7$ free-standing coating in the first heating ramp-cooling ramp in a. Four different sections can be distinguished in the first heating ramp; the first one, up to 500 °C is characterized by an elastic behavior with no deviations from a straight line. The coefficient of thermal expansion (CTE) measured in this section of the heating curve is $7.6 \cdot 10^{-1}$ °C^{-1}. From 500 to ~950 °C the heating curve presents a not linear behavior that can be related with the relaxation of the stresses accumulated in the as sprayed coatings. Then, from 960 °C to 1080 °C a sharp contraction is detected that can be related with the crystallization events discussed above. The CTE measured at this temperature was $8.5 \cdot 10^{-1}$ °C^{-1}, higher than the measured in the amorphous as sprayed coatings. Between 1150 and 1300 °C, there is a sharp increase of the relative length of the sample. This expansion can be related with the transformation of the disilicate and monosilicate metastable phases to the corresponding high temperature stable phases shown in Raman analysis (Fig. 19).

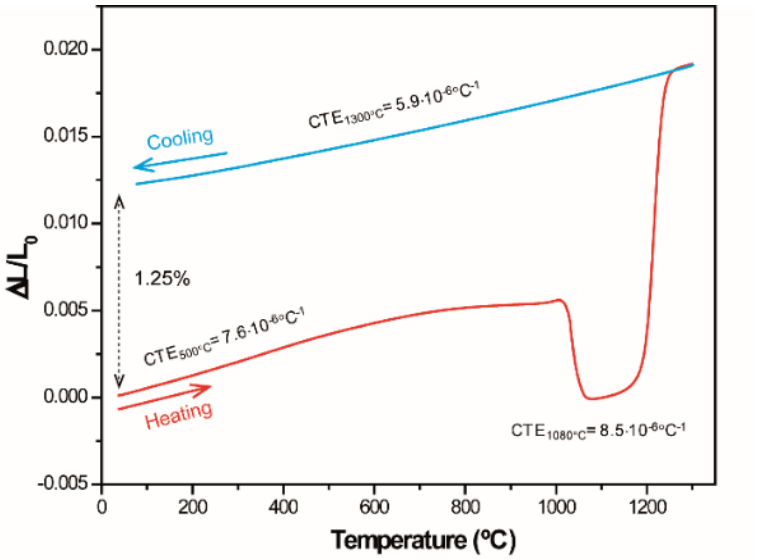

Figure 20. Relative thermal expansion with temperature. Coefficients of thermal expansion (CTE) measured after heat treatments at specific temperatures and residual expansion after test are also shown in the figure.

This expansion, observed just in the first heating-cooling tests, and the fact that the top coat coating is constrained by the underlying Si/SiC architecture coatings, maybe the responsible for the closing of the microcracks present in the as sprayed coatings when the system is heat treated above the transformation temperature ~ 1220 °C.

The effect of thermal treatment on the coating hardness was explored with micro-indentation techniques. The tests were performed in CIATEQ-CIDESI facilities. The insets in Figure 21 show the Vickers hardness of the as-spray coating specimen as a function of load and the indentation footprint of a 3N test. The highest hardness value was obtained with the lowest load of 2 N, which may correspond to the elastic recovery of the material as has been observed in other studies with ceramic materials. The loads 3, 5 and 10 N presented very similar hardness values, which agree with some studies performed on ceramic materials where at higher indentation loads, hardness-load curves flatten out and hardness becomes constant (plateau). However, at a load of 3N, a transition point can be observed, which is associated with the onset of fracture in the vicinity of the indentation. Hence, in this study 3N was the load chosen to make the measurements of hardness in the as-spray and heat-treated specimens. Figure 21 shows the Vickers hardness measured under these conditions on the as spray coating and on heat treated coatings at 1080 and 1300 °C. The hardness shows an abrupt increase of the values measured from amorphous to crystalline coatings. The hardness of the as sprayed coating was 4.5 GPa and increased to 6.1 GPa for the coating heat treated to 1080 °C and to 6.4 GPa for that heat treated at 1300 °C, which means an increase of ~ 40%.

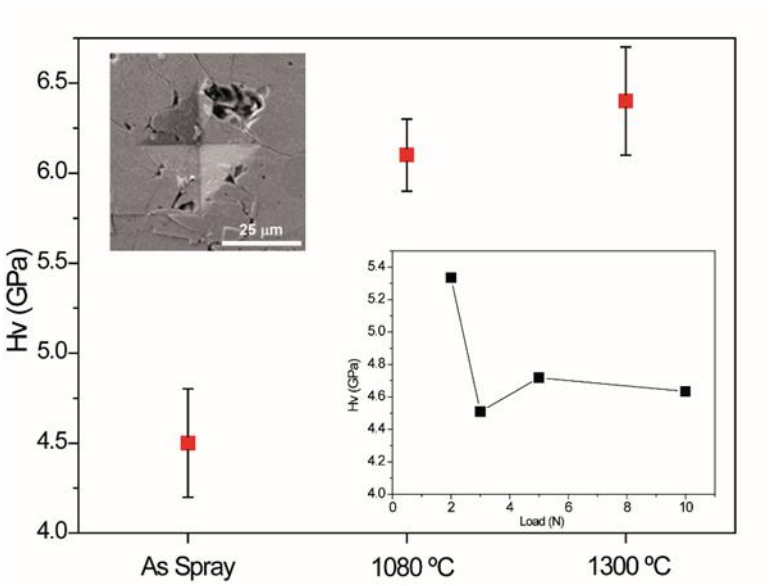

Figure 21. Vickers hardness (Hv) measured on the coatings heat treated at different temperatures. The inset images show the Load/Hardness tests performed on as sprayed coating to choose the right load for the measurement and one indentation footprint obtained with 3N load.

One of the objectives for 2nd year was testing the EBC architectures in the Burner-Rig set up employed in the 1st year of the project to test the TBCs. Before subjecting the EBCs to a such aggressive test we decided to evaluate if the presence of Yb-monosililcate and disilicate phases with different thermal expansion coefficient could compromise the EBC performing cycling tests were in a furnace between 200 and 1200 °C at a heating/cooling rate of 10 °C·min^{-1} (200 cycles). Figure 22 shows different magnifications and areas of the cycled coating microstructure. The low magnification images of Fig. 22a and 22b show that no vertical cracks running through the entire coating were detected, even though the thermal expansion coefficient of the Yb_2SiO_5/Yb_2Si2O7 coating is ~ 30% higher than that of Si bond coat ($4.6\cdot10^{-6}$ °C^{-1}) and SiC substrates ($4.02\cdot10^{-6}$ °C^{-1}). The most evident effect of the thermal cycling test is the growth of grain structures (Fig. 22c) and the formation of an oxidation scale between the Yb_2SiO_5/$Yb_2Si_2O_7$ top-coat and the Si bond coat (Fig. 15d). It is well known that the oxidation scale is SiO_2. In this case the average thickness is just ~3 µm. The reduction of the thickness of this scale could be obtained by increasing the coating thickness but that could increase the thermal stresses in the outer layers of the topcoat causing the initiation of vertical cracks that could run through the entire coating. The multilayer will allow to increase the total thickness of the coting without causing the spallation of the coating. For this purpose, the number of layers and maximum CTE (i.e. highest amount of Yb_2SiO_5) must be optimized for a stablished thickness of the coating.

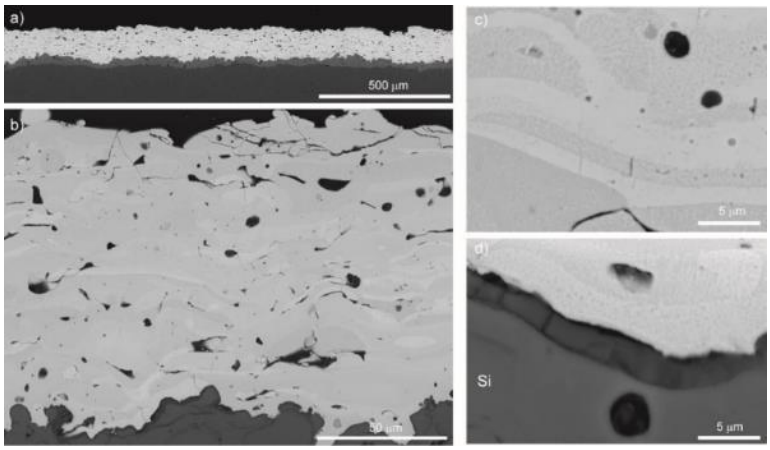

Figure 22. Cross section of cycled coating a) low magnification cross-section of the coating showing no vertical cracking, b) microcracks are detected mainly at the top of the coating, b) high magnification images show microcracks in "bright" splats, c) SiO_2 scale between top-coat and Si bond-coat.

This collaboration work resulted in the publication of the paper **E.Garcia, O.Sotelo-Mazon, C.A.Poblano-Salas, G.Trapaga, S.Sampath, Characterization of $Yb_2Si_2O_7$–Yb_2SiO_5 composite environmental barrier coatings resultant from *in situ* plasma spray processing, Ceramics International 46 (2020) 21328-21335.** https://doi.org/10.1016/j.ceramint.2020.05.228

One-Layer EBCs were tested in the Burner Rig at CTSR (Figure 5). The coatings were heated with the torch up to the surface temperature of the top-coat EBC reached 1100 °C, the melting point of the Calcium Magnesium Aluminum Silicate composition (CMAS Ash) powder selected for this test. Then CMAS powder was injected during 10 s in the flame and projected towards the EBC surface. Figure 23 shows images of the EBC surface just before the CMAS was injected in the flame, 15 s and 15 min after. The plot of temperature vs. time recorded on the EBC surface by optical pyrometry and at the back of the SiC substrate by a thermocouple are also shown in the same figure. It worth to notice that the molten CMAS droplets were pushed to the edges of the sample during the test by the stream of high temperature gases coming from the Burner-Rig torch.

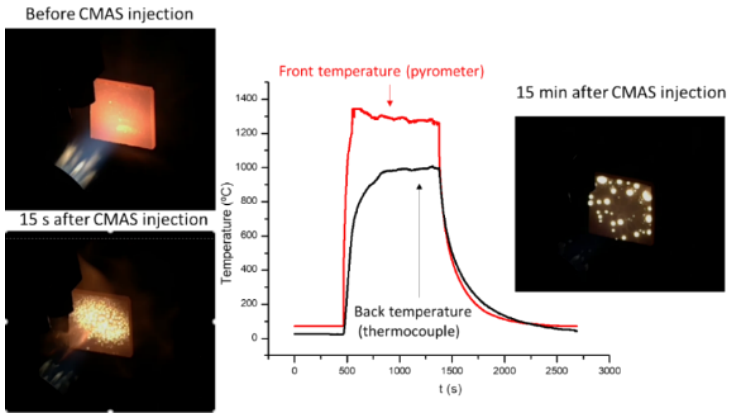

Figure 23. Images of EBC top surface at different time of the Burner-Rig-CMAS test and the temperature vs. time curves recorded for the EBC top surface and the back of the SiC subtrate

The SEM inspection of the tested EBC reported the images shown in Figure 24. The top surface showed areas with dark phase related with low density CMAS (top surface left). In this area are detected round features/surface pores related with the bursting of glass bubbles formed by the impingement of hot gases on the high temperature-low viscosity glass melt. In the areas beneath the glass an extensive grain growth is detected (top surface left). The micrographs taken in the cross-section of the coating revealed that the CMAS glass crystallized in some extension after the cooling down. Higher magnification micrographs (EBC cross-section left) showed the incipient decomposition of the top surface of the coating. Undoubtedly, longer test are needed to identify the top coat decomposition/depletion kinetics and how this is affected by the composition of the top most layer of the EBC structure, but undoubtedly this test showed that adhesion of the different layers of the EBC system is enough to avoid the spallation of a ceramic coating deposited on a such a rigid substrate as SiC.

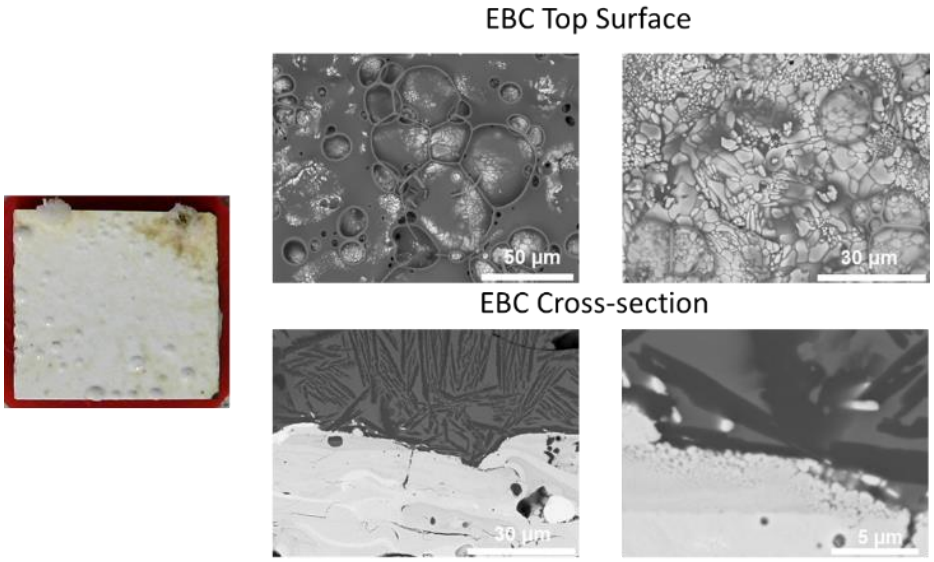

Figure 24. Optical image of the EBC sample after Burner-Rig-CMAS test and SEM microphotographs at different magnification of the EBC topcoat and cross-section

Three different coatings were produced on Si coated SiC substrates following the idea of increasing the Yb_2SiO_5 content modifying the plasma spray conditions. Figure 25 shows the as sprayed and heat-treated cross sections of three monolayer coating named 3H, 4.5H and 6H. The Yb_2SiO_5 content in each of them was: C1=22 vol%, C6= 40 vol% and 6H: 84 vol%. The as sprayed microstructure was similar to every of them (see Figs. 25 a,b and c), but the heat treatment had different effect. It is clear from Figs. 25 d,e and f that the higher the Yb_2SiO_5 content the more evident the presence of vertical cracks is.

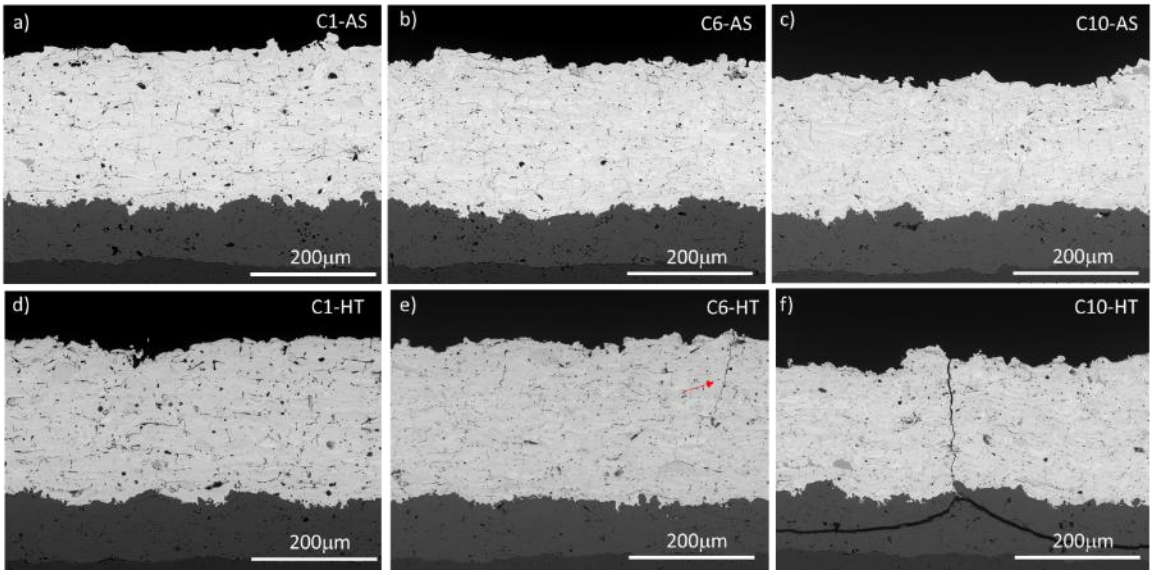

Figure 25: SEM cross-section views of As sprayed monolayer coatings C1-AS (a), C6-AS (b) and C10-AS (c) and the corresponding heat treated coatings C1-HT (d), C6-HT (e) and C10- HT (f). Red arrow in e) shows the presence of a crack.

To minimize the crack formation CTSR explored the deposition of multilayer structures with different thermal expansion coefficient of each layer by modifying the plasma spraying parameters (mainly the power and the H_2 content of the plasma) and thus the chemistry of each coating (SiO_2 content) what is related with Yb_2SiO_5 and the increasing of CTE. Figure 26 shows another example of the fruitful collaboration with our partners in Mexico. We sprayed the coatings using three different spraying conditions without changing the feedstock powder and them at CINVESTAV facilities analyzed the chemistry of the coatings by EDS, finding that the SiO_2 content is lower at the top of the coating (where the Highest power and H_2 content was used) than at the middle or the bottom where milder spraying conditions were used.

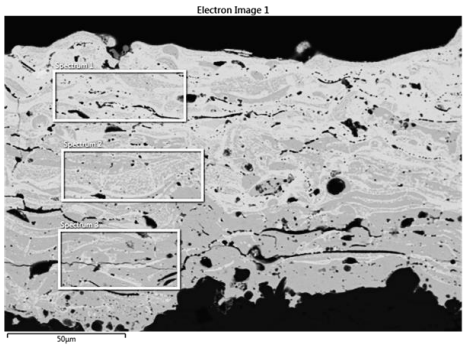

Spectrum Label	Spectrum 1	Spectrum 2	Spectrum 3
O			
SiO2	15.99	19.42	22.10
Yb2O3	84.01	80.58	77.90
Total	100.00	100.00	100.00

Figure 26. Cross-section of multilayer EBC and EDS analysis obtained at depths where different spraying conditions were used.

The graded Si content is appreciated in Figure 26 that shows a mapping of the different elements. The lower the SiO_2 content the higher the coefficient of thermal expansion measured by

dilatometric techniques. This is an indication that more Yb_2SiO_5 is present in the top part of the coatings which is a benefit for the water vapor corrosion resistance of the system as the volatilization of Yb_2SiO_5 in those environments is lower than that of $Yb_2Si_2O_7$

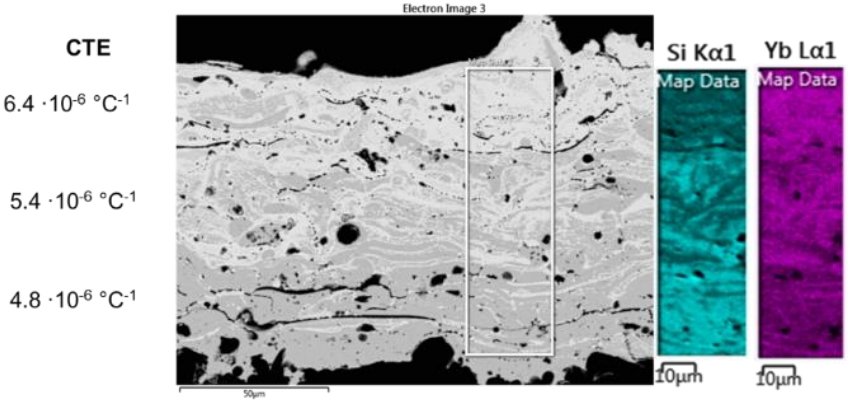

Figure 26. Cross-section of multilayer EBC and EDS map analysis of Si and Yb with the CTE measured by dilatometric analysis of freestanding thick coatings

The preliminary study performed by or colleagues from CIDESI, Mexico concerning the stress evolution during the first cycle of a $Yb_2SiO_5/Yb_2Si_2O_7$ free-standing coating/substrate coating system presented in the Report of the second year was extended to each layer of the multilayer EBC of 5 layers with graded value in Coefficient of Thermal Expansion (CTE) presented in Figure 27a. In these calculations were considered not only the CTE values for the coatings with the different compositions but the actual thermal expansion curves of each layer measured in the freestanding coatings prepared at CTSR (Fig. 27b). The curves obtained for samples machined from SiC substrates and freestanding thick coatings of Si bond coats (Fig. 27c) were also used for the modeling.

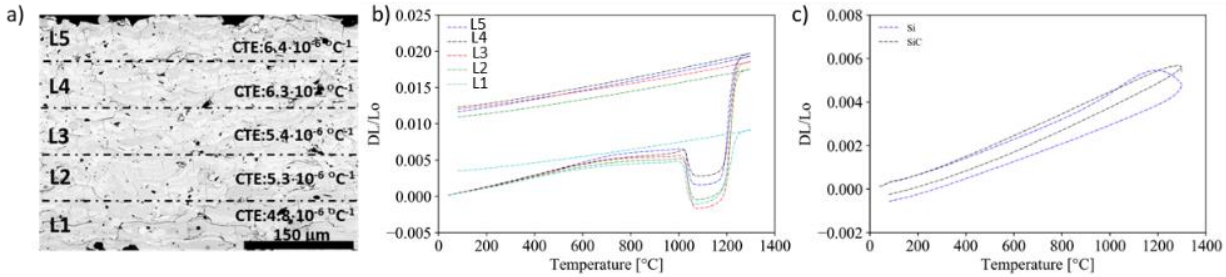

Figure 27. Functionally graded disilicate- monosilicate multilayer, multifunctional coating synthesized at CTSR Strony Brook with associated thermal expansion data for each layer. This data has been provided to CONACYT researchers in Mexico for analytical modeling which is explained below.

With these data CIDESI obtained the predictions for the evolution of thermal stress with temperature for the different YbDS layers (different composition of $Yb_2SiO_5/Yb_2Si_2O_7$) in a Si-SiC-YbDS EBC. These predictions provided preliminary insight regarding the crack healing and vertical cracking processes observed in the EBC during first heating from the amorphous as-sprayed state. The curves in Fig. 4a show that, notwithstanding its composition, the YbDS layer is subjected to a compressive state of thermal stress during heating from room temperature up to 1000 °C. In this

temperature range, the magnitude of the compressive state of thermal stress exhibits three stages. First, the magnitude increases at a quasi-constant rate for temperatures in the range of room temperature to 600° C. Next, the magnitude of the compressive state of stress continues to increase with a gradual rate reduction for temperatures between 600 and 700 °C. Afterwards, the magnitude of the compressive thermal stress reduces with increasing temperature from the value prevailing at 700 °C. The compressive thermal stress state operating from room temperature to 1000 °C provides favorable conditions for the micro-crack healing. in heat treated YbDS-6H samples. At 1000 °C, the state of stress in the YbDS layer changes from compression to tension in a sudden manner. The magnitude of this tensile state of stress equals or exceeds its compressive counterpart prevailing at temperatures slightly below 1000 °C. The onset of vertical cracking in the coating could be attributed to this abrupt change in the state of stress. From 1000 to 1200°C, the level of tensile stress remains practically constant. At 1200 °C the state of stress exhibits another sudden reversal from tension to compression. The magnitude of the new state of compressive stress is about three times that corresponding to the tensile stress state. Further heating from 1200 to 1300 °C results in a modest increment in the compressive thermal stress magnitude. Finally, cooling the EBC from 1300 to 80 ° C results in a small (if not negligible) and quasi-linear reduction in the magnitude of the thermal stress. This situation provides a persistent state of compressive thermal stress that could assist crack healing during EBC cooling.

Linear extrapolation of the cooling segment of the thermal stress curves shown in Fig. 28a towards room temperature suggest that, for all compositions, a residual stress is present in the YbDS layer at the conclusion of the thermal cycle. This residual stress is different from that operating in the as sprayed amorphous cool state at the beginning of the thermal cycle. Figure 28b plots the value of the residual stress for each of the layers of EBC shown in Figure 27a.

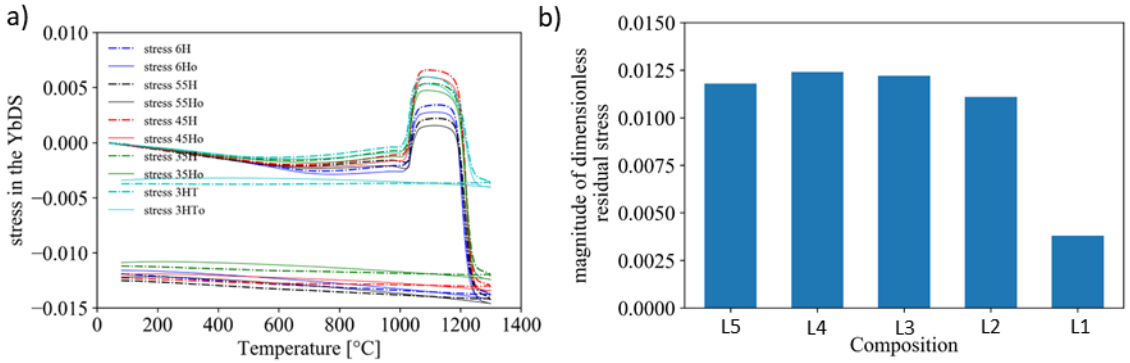

Figure 28. Dimensionless thermal stress in the EBC YbDS layers calculated by Dr. Miguel Jimenez of CIDESI. a) Evolution of stress with temperature (in dimensionless form) for a 5 Ytterbium Disilicate compositions. b) Magnitude of the compressive residual thermal stress in the Ytterbium Disilicate layer at the end of the first cycle as suggested from the curves in panel a).

The last year of the project CTSR used these results to work on the developing multilayered coatings formed by different number of layers that maximized the amount of Yb_2SiO_5 in the top layers minimizing the crack formation. Table I shows the different conditions employed for spraying the different layers the composition of each layer (5 specific layers) in terms of Yb_2SiO_5 and $Yb_2Si_2O_7$ vol% content and the thermal expansion coefficient measured by dilatometric techniques. Three multilayer architectures produced in this study: 3L, 5L and 10L. The coatings with different Cx

composition were produced in-situ varying dynamically the spraying parameters. The thickness of the different layers forming the composition was controlled by the number of passes. For a target of a total thickness of 260-270 μm, the FGM EBCs were designed to be ~180 μm of low CTE/YbMS content, ~60 μm of intermediate CTE/YbMS content and ~30 μm high CTE/YbMS content.

Table I. Conditions employed for the preparation of multilayer coatings

Condition	Ar (slpm)	H_2 (slpm)	I (A)	P (kW)	$Yb_2Si_2O_7$ (vol%)	Yb_2SiO_5 (vol%)	CTE ($x10^{-6}\,°C^{-1}$)
C1	50	3	380	29.7	78	22	4.74
C2	50	3	410	32.6			
C3	50	3.5	410	33.7	61	39	5.30
C4	50	3.5	430	35.5			
C5	50	4	430	35.5			
C6	50	4.5	430	37.1	60	40	5.36
C7	50	4.5	460	39.7			
C8	50	5	460	40.3			
C9	50	5.5	460	40.8	23	77	6.27
C10	50	6	500	45.8	16	84	6.33

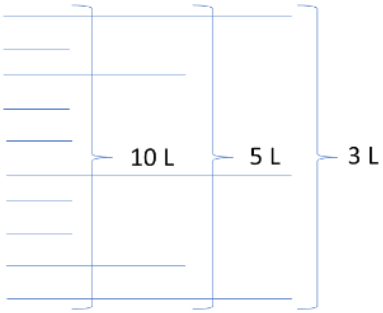

Figure 29 shows the microstructure of the FGM EBCs architectures in the as spray and after performing the crystallization heat treatment for coatings crystallization. None of the as sprayed coatings shows vertical cracks running through the coating, just, as in the case of monolayer coatings, a network of microcracks that is reduced after the crystallization heat treatment. The three multilayer architectures present thin vertical cracks (pointed with a red arrow in Figs. 29d, e and f). The vertical cracks run the equivalent distance to the coatings with higher (C10) and intermediate (C6) content, this is clearly seen in 3L EBC. Similar behavior is seen in 5L and 10L architectures. Where the crack stops at similar distances from the top. It must be pointed out that even the presence of vertical cracks is not avoided in the proposed FGM architectures, the length has been drastically reduced when compared with the monolayers shown above. Taking into account that at least 30 microns of the FGM top layer are formed by a coating system with YbMS contents higher than 77 vol%, which is expected to work better that high content YbDS coatings in water vapor combustion environments.

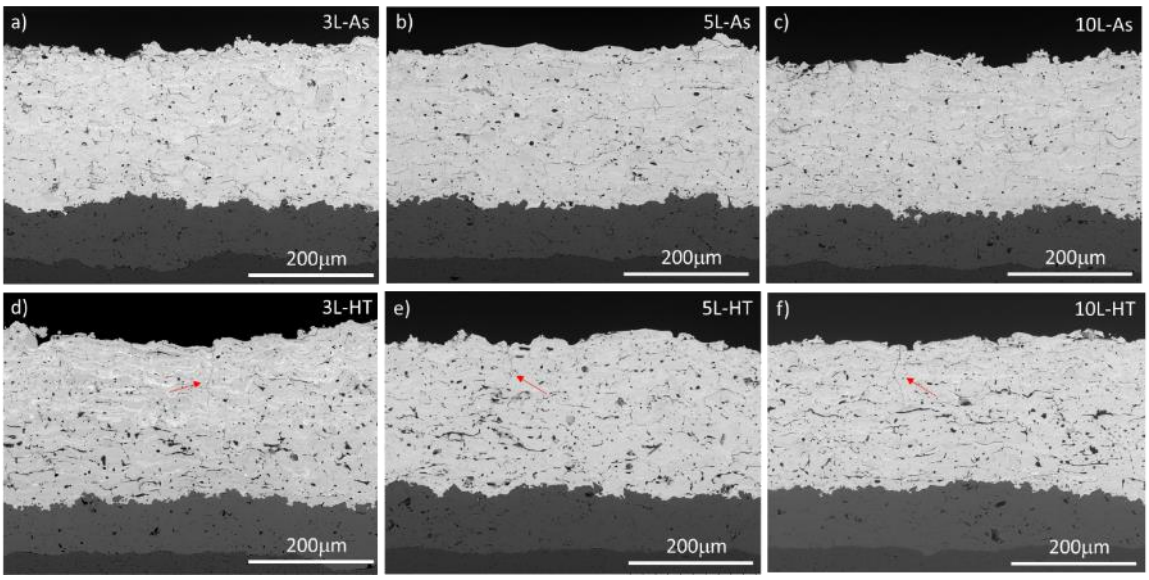

Figure 8: SEM cross-section views of as sprayed multilayer EBCs, 3L-AS (a), 5L-AS (b) and 10L-AS (c) and the corresponding heat-treated systems 3L-HT (d), 5L-HT (e) and C10- HT (f). Red arrows in

IMPACTS

The collaboration work performed inside the scope of this project has brought new approaches to testing the performance of multilayer Thermal and Environmental Barrier coatings in simulated combustion environments with the addition of CMAS attack. It has highlighted the importance of the top coat characteristic (porous, DVC, dense..) in the dynamics of the molten CMAS on the high temperature surface of the TBC/EBC and its penetration/reaction with that surface and the distribution of cracks present in the coatings. Numerical and FEM models have been used to improve the design of the TBC and EBC multilayer coatings. Optimized thicknesses of the different layers were proposed and, for EBCs revealed the thermomechanical stresses generated during the heat treatments that must be performed for recovering the crystallinity after plasma spraying of the coatings. Advanced techniques like CT-SCAN have been employed to elucidate the 3D distribution of cracks in a multilayer TBC system which is paramount to forecast the CMAS penetration in tested systems. The same technique was tested positive to observe the presence of this glassy layer on a tested TBC. Concerning the study of Environmental Barrier Coatings, the advances done during the collaboration project have been more than significant. First, it was developed a heat treatment to recover the crystallinity of the amorphous as sprayed coatings and the evolution of phases, from metastable to stable ones was identified and explained using different advanced techniques like Raman Spectroscopy and High Temperature XRD analysis. It was observed and described the paramount effect of the spraying conditions on the chemical composition of the Yb-Sililcate EBC coatings, which intimately related with the amount of Yb-Disilicate ($Yb_2Si_2O_7$) and Yb-Monosilicate (Yb_2SiO_5) present in the coatings and thus its thermomechanical and chemical properties. This effect was used to prepare in-situ multilayer Environmental Barrier Coatings with a gradient in $Yb_2Si_2O_7$/ Yb_2SiO_5 ratio from the bottom to the top that are expected to perform better in water vapor atmospheres due to the high content of Yb_2SiO_5 phase in the top layer and that minimize the

presence of cracks due to the gradient coefficient of thermal expansion (CTE) created with this new design.

CHANGES

Much of 2020 was affected by Covid. Due to our location in NY, our facility was shut down for about 4 months following which there was gradual opening over several months. However, the team managed to get significant productivity through remote work, data analysis etc. Since early fall work has resumed and barring some set back in the end of year, work is starting to operate in steady state. However, there was no possibility for face to face interactions with our Mexican partners and also work is yet to resume in Mexico at a reasonable pace for collaboration. AFOSR provided a no cost extension for 1 year

ADDITIONAL INFORMATION

Personnel Exchange and Logistics:

The 3 + 1 years of the project revealed a good personnel collaboration between the two teams. This collaboration was evidenced not only by the results described in this final report but also by other activities like the Skype conferences performed at least once every 2 months that summoned the teams to discuss the general advancements on the project and the status of specific activities. This allowed the expanded group of researchers from both organizations to interact. Different CONACYT researchers, attended and presented at the Stony Brook Industrial Consortium for Thermal Spray Technology meetings in 2018 and 2019. Stony Brook post-doc and graduate students made trip to Mexico to both familiarize with characterization equipment and participate in experiments supplying to Mexico samples produced at Stony Brook. Prof. Sampath participated in the 2019 SOARD Program Review held in Santiago de Chile, Chile and Dr. Eugenio Garcia participated in the workshop Advanced Defense Materials Research in the XXVIII International Materials Research Congress held in Cancun, Mexico. Due to the COVID-19 pandemic it was no personnel exchange in years 2020 and 2021 but the contact between the two teams was fluent using online tools. Samples were sent by mail instead bringing with us in the yearly visit we use to pay our colleagues in Queretaro or when they visited our facilities for the conferences we organize in spring and fall.

Outreach of results

Papers

1. E. Garcia, Hwasoo Lee, Sanajay Sampath “Phase and microstructure evolution in plasma sprayed Yb2Si2O7 coatings” 39 (2019) 1477–1486. https://doi.org/10.1016/j.jeurceramsoc.2018.11.018

2. E. Gildersleeve, S. Sampath. "Dynamic interactions of ingested molten silicate particles with air plasma sprayed thermal barrier coatings." *Journal of Materials Research* 35.17 (2020): 2321-2334. https://doi.org/10.1557/jmr.2020.196

3. E.Garcia, O.Sotelo-Mazon, C.A.Poblano-Salas, G.Trapaga, S.Sampath, Characterization of $Yb_2Si_2O_7$–Yb_2SiO_5 composite environmental barrier coatings resultant from *in situ* plasma spray processing, Ceramics International 46 (2020) 21328-21335. https://doi.org/10.1016/j.ceramint.2020.05.228
4. S.V. Shinde, S. Sampath. "Interplay between Cracking and Delamination in Incrementally Deposited Plasma Sprayed Coatings."*Acta Materialia* 215 (2021): 117074. https://doi.org/10.1016/j.actamat.2021.117074
5. E. Garcia, H. F. Garces, L. R. Turcer, H. Bale, N.P. Padture, S. Sampath, "The Crystallization Behavior of Air-Plasma-Sprayed Ytterbium-Silicate-Based Environmental Barrier Coatings" Journal of the European Ceramic Society 41 (2021) 3696-3705. (https://doi.org/10.1016/j.jeurceramsoc.2020.12.051)
6. S.V. Shinde, S. Sampath." Factors Governing Segmentation Crack Characteristics in Air Plasma Sprayed Ceramics." *Journal of the European Ceramic Society* 42 (2022) 1077-1087 https://doi.org/10.1016/j.jeurceramsoc.2021.10.064

Conferences:

1. **42nd International Conference and Exposition on Advanced Ceramics and Composites January 21 - 26, 2018 Daytona Beach, Florida**
   - **1.1** E. Garcia Granados; H. Lee; S. Sampath Processing effects on characteristics of rare-earth silicates for considerations as environmental barrier coatings for ceramic composites
   - **1.2** Edward J. Gildersleeve and Prof. Sanjay Sampath Examining the Role of Process Induced Porosity Differences on CMAS Interactions in Plasma Sprayed Thermal Barrier Coatings
2. **INTERNATIONAL THERMAL SPRAY CONFERENCE AND EXPOSITION (ITSC 2018) May 7-10, 2018 Orlando, Florida**
   - **2.1** Eugenio Garcia Mr. Hwasoo Lee, Sanjay Sampath "Plasma Sprayed Yb2Si2O7 as an Example of Rare-Earth Silicate for Environmental Barrier Coatings Application– Processing Effects on Coating Features"
   - **2.2** Edward J. Gildersleeve and Prof. Sanjay Sampath "Capturing Process Subtleties in the Processing of Thermal Barrier Coatings for Complex Geometries"
   - **2.3** Edward J. Gildersleeve and Prof. Sanjay Sampath "Process-Property-Performance Relationships of YSZ and GDZ Air Plasma Sprayed Thermal Barrier Systems Regarding CMAS Attack
3. **SPRING MEETING OF THE CONSORTIUM OF THERMAL SPRAY June 20-21st, 2018, Stony Brook University, NY**
   - **3.1** Edward Gildersleeve, Gerardo Trapaga "CTSR Multilayer Review & Current Activities AFOSR-CONACYT collaboration Project
   - **3.2** Eugenio Garcia, Phase and Microstructural Evolution of APS YbSi EBC
4. **43rd International Conference and Exposition on Advanced Ceramics and Composites January 27 – February 1st , 2019 Daytona Beach, Florida**

4.1 E. Garcia Granados; F. Caliari, H. Lee; S. Sampath Implications of rapid quenching and chemical composition shift in Plasma Sprayed Yb2Si2O7 Environmental Barrier Coatings

4.2 Edward J. Gildersleeve and Prof. Sanjay Sampath Process-Induced Architectural Variations in Plasma Sprayed Thermal Barrier Coatings and Their Implications on Performance in a Thermal Gradient Environment with and Without Siliceous Debris

5. **Oerlikon-Metco Headquarters, Wohlen, Switzerland. Edward Gildersleeve, Failure Mechanisms in Plasma Sprayed Thermal Barrier Coatings (Invited Talk)**

6. **SPRING MEETING OF THE CONSORTIUM OF THERMAL SPRAY June 11-13st, 2019, Stony Brook University, NY**

   6.1 S. Sampath, Multilayer Thermostructural Coating Systems, The Why, What and How

   6.2 E. Gildersleeve, Multilayer Synthesis and Fabrication Capabilities and Challenges

   6.3 Miguel Jimenez (Mexico), Juan Alvarado (Mexico) Alfredo Valarezo (Ecuador), Complementary Latin American Efforts through AFOSR-Conacyt Mexico Project

   6.4 Josh Margolies (GE) Eugenio Garcia, Bruce Pint (ORNL), Environmental Barrier Coatings: Science and Technology Linkages.

7. **S. Sampath, E. Garcia-Granados, GT2019-91750 Processing Science of Thermal and Environmental Barrier Coatings ASME 2019 TURBOEXPO, June 17-21 Phoenix Arizona (Invited)**

8. **E. Garcia, E. Gildersleeve, F. Caliari, S. Sampath, O. Sotelo, C. Poblano, G. Trapaga, In-situ Plasma Spray Processing of $Yb_2Si_2O_7$ Function Graded Material (FGM)-Environmental Barrier Coatings (EBCs), XXVIII International Materials Research Congress, 2019 Cancun, Mexico.**

9. **FALL MEETING OF THE CONSORTIUM OF THERMAL SPRAY November 13th, 2019, GE Power, Schenectady, NY.**

   9.1 E. Garcia, Effect of Plasma Gas Chemistry and Plasma Type on the Composition of Silicate EBC Coatings

   9.2 E. Gildersleeve, Microstructure Effects on CMAS response of TBCs

10. **44th International Conference and Exposition on Advanced Ceramics and Composites January 26 - 31, 2020 Daytona Beach, Florida**

    10.1 E. Garcia Granados; H. Lee; S. Sampath Processing effects on characteristics of rare-earth silicates for considerations as environmental barrier coatings for ceramic composites

    10.2 Edward J. Gildersleeve and Prof. Sanjay Sampath Examining the Role of Process Induced Porosity Differences on CMAS Interactions in Plasma Sprayed Thermal Barrier Coatings

11. **CTSR CONSORTIUM WEBINARS SERIES**

    11.1 S. Shinde. Interplay between Adhesion, Cracking, and Delamination in Thermal Spray Coatings. Webinar #4 - July 9

11.2 E. Gildersleeve" Influence of Substrate Geometry on the Process-Property-Performance Relationships in Air Plasma Sprayed Ceramic Coatings" Consortium Webinar #7 August 6th, 2020.

11.3 E. Garcia, "Air Plasma Spray of Silicate based Environmental Barrier Coatings (EBCs): Processing-Materials Interrelations" Webinar #8 August 13th, 2020.

12. Henry Royce Institute (United Kingdom) Webinars, Coatings and Ceramics

12.1 S. Sampath, "Thermal Spray as an Additive and Layered Manufacturing Technology For Applications In Energy Systems" September 9th, 2020.

13. Surface Engineering for Advanced Materials (SEAM) Webinar Series, Australian Research Council Industrial Transformation Training Centre

13.1 S. Sampath "Thermal Spray as an Additive and Layered Manufacturing Technology for Applications in Energy Systems" October 14th, 2020

14. ITSC 2021, Quebec City, Canada, 2021 24-28 May, 2021. (On line)

14.1 S.V. Shinde, S. Sampath. "Correlations Between Stress Distributions and Coating Adhesion Strength as Tested by Tensile Adhesion Methods"

14.2 E. Garcia, E. Gildersleeve, S. Sampath "Effect of Plasma Characteristics on the Composition and Properties of Silicate Environmental Barrier Coatings"

15. CTSR Consortium Webinar (2021)

15.1 E. Gildersleeve, S. Sampath "Thermal Cyclic Testing of Thermal Barrier Coatings; Nuances and Considerations" CTSR Consortium Webinar (2021)

Awards

1. **Oerlikon-Metco Young Professionals Award at ITSC 2018**
   Edward Gildersleeve ""Process-Property-Performance Relationships of YSZ and GDZ Air Plasma Sprayed Thermal Barrier Systems Regarding CMAS Attack"
2. **Oerlikon-Metco Young Professionals Award at ITSC 2019**
   Shalaka Shinde "Segmentation Crack Formation Dynamics"
3. **Prof. Sampath received the prestigious John Jeppson Award from American Ceramic Society in 2019**
4. **Prof. Sampath received the ASM International Albert Sauveur Achievement award for 2020.**